Polarization-based perturbations to thermopower and electronic conductivity in highly conductive tungsten bronze structured (Sr,Ba)Nb_{2}O_{6}: Relaxors vs normal ferroelectrics

Jonathan A. Bock, Susan Trolier-McKinstry, Gerald D. Mahan, and Clive A. Randall

Phys. Rev. B **90**, 115106 — Published 2 September 2014

DOI: 10.1103/PhysRevB.90.115106

Polarization-Based Perturbations to Thermopower and Electronic Conductivity in Highly Conductive Tungsten Bronze Structured $(Sr,Ba)Nb_2O_6$: Relaxors vs Normal Ferroelectrics.

Jonathan A. Bock, Susan Trolier-McKinstry, G.D. Mahan and Clive A. Randall
Center for Dielectrics and Piezoelectrics, Materials Research Institute, Penn State University, University Park, Pa 16802, USA

Abstract

Electrical conductivity, thermopower, and lattice strain were investigated in the tetragonal tungsten bronze structured $(Sr_x,Ba_{1-x})Nb_2O_{6-\delta}$ system for $0.7>x>0.4$ with large values of δ. These materials show attractive thermoelectric characteristics, especially in single crystal form. Here, the Sr/Ba ratio was changed in order to vary the material between a normal ferroelectric with long range polarization to relaxor behavior with short-range order and dynamic polarization. The influence of this on the electrical conduction mechanisms was then investigated. The temperature dependence of both the thermopower and differential activation energy for conduction suggests that the electronic conduction is controlled by an impurity band with a mobility edge separating localized and delocalized states. Conduction is controlled via hopping at low temperatures, and as temperature rises electrons are activated above the mobility edge, resulting in a large increase in electrical conductivity. For relaxor ferroelectric based compositions, when dynamic short-range order polarization is present in the system, trends within the differential activation energy and thermopower show deviations from this conduction mechanism. The results are consistent with the polarization acting as a source of disorder which affects the location of the mobility edge and, therefore, the activation energy for conduction.

Introduction

Ferroelectric materials have been of interest for multiple decades due to high electromechanical coupling coefficients, high permittivity, and high electro-optical coefficients, amongst others. These

properties make them useful for high performance capacitors, piezoelectric sensors and actuators, pyroelectric detectors, electro-optic switches, electrocaloric coolers, polarization based non-volatile memories, and multiferroic sensors and switches. [1–6] A commonality of these applications is that they require the application of a sizable electric field, and this necessitates that the ferroelectric materials be insulating. Consequently, much less attention has been paid to the application possibilities for ferroelectric materials that are electrically conducting. Previous work has found effects such as modification of the Schottky barrier at grain boundaries due to the ferroelectric polarization, and this is used in PTCR thermistors [7]. Recently, renewed interest has revolved around polarization-aided photovolatics [8–10] and thermoelectrics [11–14], conducting domain walls [15–20] and possibly metallic ferroelectricity [11,21–25].

Recent work by Kolodiazhnyi et al. [21,22], Lee et al. [11] , and Jeong et al. [25] on heavily doped $BaTiO_3$; Sergienko et al. on $Cd_2Re_2O_7$ [23]; and Shi et al. [24] has reopened investigations into metallic ferroelectrics, a topic which has been comparatively ignored since early ideas by Anderson and Blout [26] and Matthias [27]. Metallically conducting samples that show structural distortions similar to a ferroelectric have been reported [21] [24], but the most heavily studied of these, $BaTiO_{3-\delta}$, was later found to be inhomogeneous in nature [25]. Jeong et al. suggest that the Ti-O bond distortion (the polarization) and metallic conductivity originate from different volume fractions of the material. The polarization may locally be causing a transition into a semiconducting state. A full understanding of polarization/conduction interactions needs extensive work; however, it is possible that polarization may act as a local field to shift electron concentrations, change the degeneracy of the conduction band, or act as sources of disorder for Anderson localization.

In terms of thermoelectricity, ferroelectrics are interesting due to phonon scattering at domain walls [28] [29], the interaction of soft optic phonon modes with heat-carrying acoustic phonons [30,31], and the glasslike properties in relaxor ferroelectrics [28]. All of these phenomena act to lower the thermal conductivity and should lead to higher thermoelectric figure of merits. Although relaxor ferroelectricity

is beneficial for low thermal conductivity, the lack of research on conducting ferroelectrics results in little knowledge on its effect on the thermopower and electrical conductivity – the other two properties important to thermoelectric materials. Here we investigate $(Sr_x,Ba_{1-x})Nb_2O_6$ (SBNx) which has recently been shown to possess a high thermoelectric power factor on reduction. [12] The ability to transform SBN between relaxor ferroelectricity and normal ferroelectricity via changing the Sr/Ba ratio makes it an interesting system to investigate the role of polarization in conduction.

SBN is a tetragonal tungsten-bronze structured ferroelectric material, P4mm in the paraelectric phase. The basic crystal structure is made up of corner-shared NbO_6 octahedra which result in square, pentagonal, and triangular channels along the c-axis. The Sr and Ba ions sit in the square and pentagonal channels and the Sr/Ba ratio affects the (P4mm→P4/mmm transition) as well as controls if the material is a normal or relaxor ferroelectric. Normal ferroelectrics have a long range order to the polarization and sharp phase transitions, whereas relaxor ferroelectrics have random and dynamic nanosize polarized regions which are distributed in size and develop over a very broad temperature range. The distinctions between normal and relaxor ferroelectrics have been extensively reviewed over the past two decades. [32] [33] This change from normal to relaxor ferroelectric with Sr/Ba ratio permits the exploration of trends in the thermopower and conductivity with respect to the polarization's nature. SBN crystals have been shown to have impressive power factors along the c-axis of oxygen deficient crystals [12] and, alongside the low thermal conductivity [34,35], this results in very impressive figures of merit [14] for an n-type oxide semiconductor. It seems prudent then to study the conduction behavior of SBN to investigate how the polarization may play a role in the conductivity in both SBN and ferroelectrics in general.

Experimental Procedure

Polycrystalline samples of strontium barium niobate of differing Sr/Ba ratios were fabricated using solid-state reaction of $SrCO_3$ (>99.9%, Alfa Aesar), $BaCO_3$ (99.8%, Alfa Aesar), and Nb_2O_5 (99.9%,

Alfa Aesar). Powders were weighed in the required stoichiometric ratios and mixed via ball milling in ethanol with ZrO_2 media for 12 hours. The dried powders were calcined at 1200°C for 6 hours. High calcination temperatures and long calcination times are needed to homogenize the cation distribution and prevent Nb-rich or Ba-poor regions which result in abnormal grain growth, as discussed by Lee and Freer [36]. The calcined powders were ball milled for 24 hours using ZrO_2 media in ethanol and then sieved using a No. 80 mesh size. The milled powders were uniaxially pressed at 15 MPa and subsequently isostatically pressed at 210 MPa. Further precautions against abnormal grain growth were taken by using a 2-step sintering process. Pellets were first held at 1250°C to homogenize and then ramped to 1325°C to sinter. All samples were >95% dense after sintering.

Dense pellets were made electrically conducting via the introduction of oxygen vacancies. This was performed using H_2-H_2O gas mixtures to control the partial pressure of oxygen surrounding the sample during annealing. Samples were annealed using a partial pressure of oxygen of 10^{-14} atm at 1300°C for 30 hours. Cooling of the furnace was performed under a constant H_2-H_2O mixture at 15°C/min. Phase purity of annealed samples was investigated using XRD. During annealing, all samples form an NbO_2 second phase. This phase is not percolated in the microstructure and should not contribute heavily to conduction, as Nb_2O_5 which has been converted into NbO_2 via annealing at 1300°C under 10^{-14} atm only has a conductivity on the order of 10 S/cm at 700K. Annealed samples were cut into bars using a diamond saw. Electrical conductivity and thermopower were measured on polished bars of 10 x 1.5 x 1.5mm and 6x1x1mm dimensions, respectively.

Electrical conductivity measurements were performed via a four terminal technique with Ti/Pt electrodes deposited via sputtering and Ag wires attached with Ag epoxy. Electrical conductivity at temperatures below 420 K was measured in a Delta Design 9023 environmental test chamber, using an HP 4284A precision LCR meter. Higher temperature measurements were performed using a Keithley 2700 Integra series digital multimeter with leads fed into a tube furnace equipped with pH_2-pH_2O atmosphere control. Samples were measured under the same H_2 and N_2/H_2O flow rates that were used for

their annealing to minimize oxidation during measurement. It was found that the electrical conductivity magnitudes were consistent on both heating and cooling over multiple measurements, suggesting that changes in oxidation state do not have a significant role in the measurements.

Thermopower, S, of the materials was measured primarily on a SB100 thermopower measurement system by MMR Technologies from 200 to 600 K. The SB100 uses the integral method for determining the thermopower by utilizing the voltage on a reference sample to determine the temperature gradient over the sample of interest. A heater is utilized to change the temperature gradient over both the sample and reference material, and the Seebeck voltage is calculated using two different applied temperature gradients. One 5×5×20mm sample of SBN0.6 was measured using a ZEM-3 system at NASA Glenn Research Center. The ZEM-3 system uses the differential method for measurement of thermopower. In this method, thermocouples are used as voltage leads so that the temperature gradient can be measured directly at the voltage measurement position. An internal heater sweeps the temperature gradient and the thermopower is calculated using the slope of the ΔV vs ΔT plot. Good correlation exists between the MMR and ZEM-3 measurement systems; the ZEM-3 system has a lower noise floor, as well as the capability for higher temperature measurements and atmosphere control. The SBN0.6 sample was measured under a 0.1atm He atmosphere up to 750K. Above 750K sample reoxidation became problematic as even ultra high purity He cylinders can have partial pressures of oxygen ~10^{-7} atm which is high compared to the pO_2 used in this study for annealing samples: 10^{-10} to 10^{-16} atm.

Lattice parameters as a function of temperature were measured on $(Sr_{0.61},Ba_{0.39})Nb_2O_6$ samples annealed at 10^{-14} atm and then crushed into powder form. The powder was placed into a 1 mm quartz capillary. A vacuum was pulled on the capillary and was then backfilled with 1% forming gas. The cycle of evacuation and backfilling with forming gas was repeated >10 times and then, while under an atmosphere of forming gas, wax was melted in the quartz capillary to seal off the capillary. Temperature dependent lattice parameters were then measured using a custom-built furnace on APS beamline 6-ID-D, using NIST standard reference material 674a alumina as an internal standard to correct for temperature

variations by using the thermal expansion data measured by Brown et al. [37] Lattice parameters were used to calculate the c/a ratio in the material. The Burns' temperature (T_{Burns}) was found by identifying the deviation in the c/a ratio on cooling. This deviation is expected for relaxor ferroelectrics, due to the onset of polarization fluctuation's contribution to strain, given by $x_i = Q_{ij}\overline{P_j^2}$ where x_i is strain, Q_{ij} is the electrostrictive coefficient, and $\overline{P_j^2}$ is the average magnitude of the short-range order polarization in the system [38]. Q_{ij} for SBN0.75 are $Q_{31} = 0.71x10^{-2}\, {m^4}/{C^2}$ and $Q_{33} = 3x10^{-2}\, {m^4}/{C^2}$ [39].

Results and Discussion

The electrical conductivity of $(Sr_x,Ba_{1-x})Nb_2O_{6-\delta}$ as a function of temperature is shown for x=0.4, 0.5, 0.6, and 0.7 in Figure 1. All samples show semiconducting ($d\sigma/dt$>0) behavior at low temperatures and a trend toward metallic-like behavior ($d\sigma/dt$ <0) at high temperatures. The phrasing 'metallic-like' is used only to describe that $d\sigma/dt$ <0 and does not necessarily mean the Fermi Energy (E_F) is located in delocalized electronic states, as in a true metal. The maximum conductivity for SBN x=0.4, 0.5, and 0.6 samples occur around 680K, while the maximum for x=0.7 was outside the measurement range, >900K. It has been reported previously that in samples of SBN0.6 annealed identically to this work, the maximum in conductivity coincides with T_{Burns}. [14] This was used to hypothesize that the polarization could suppress metallic conduction, and a possible mechanism involving a spatially heterogeneous mixture of paraelectric metallic and ferroelectric semiconducting phases controlled the electronic conduction, similar to ideas put forward for $BaTiO_{3-\delta}$ [25]. Although the maximum conductivity in x=0.4, 0.5 and 0.6 occur near T_{Burns} as measured in stoichiometric compositions [40], the maximum conductivity of x=0.7 is at much higher temperatures, inconsistent with the idea that the conductivity maxima is fundamentally linked to T_{Burns}. This line of thinking also requires the assumption that the Burns temperatures in samples do not vary significantly under the presence of large numbers of oxygen vacancies and free electrons. To check the validity of this assumption, temperature dependent lattice parameters were taken on beam-line 6-ID-D at the Advanced Photon Source, Argonne National Laboratories. The measured c/a ratio of a

SBN0.6 samples is shown in Figure 2. At temperatures above T_{Burns}, the c/a ratio remains roughly constant, but there is a decrease in the c/a ratio on cooling starting at ~625K. This decrease is associated with the electrostrictive coupling of polarization to lattice strain. As the nanopolar regions are formed, the polarization along the c-axis causes both the *c* and *a*-axis lattice parameters to increase due to electrostriction [39]. Although the electrostrictive coefficient Q_{33} is larger than the Q_{13} coefficient, the larger a-axis lattice parameter (a=12.44 vs c=3.96 at room temperature) makes the c/a ratio decrease on cooling, as can be seen in Figure 2 below ~625K. As temperature is lowered further, an increase in the c/a ratio occurs below 450K and is associated with the immobilization of mesoscale polar nanoregions as described elsewhere. [41] Thus, T_{Burns} for this oxygen deficient SBN has been confirmed to be 625 ± 25K, which is comparable to the T_{Burns} in stoichiometric samples of 600K ± 25K [39] and therefore appears to be essentially invariant to the reduction condition. Therefore, the Burns temperature does not seem to be heavily dependent on carrier concentration and the burns temperature from stoichiometric compositions can be assumed to be correct in further analysis. This is in contrast to the curie temperature in normal ferroelectrics, which has been shown to be dependent on carrier concentration [42] [11].

Another explanation for the maximum in conductivity could be carrier freeze-out. If carrier freeze-out is occurring in SBN, then changes in carrier concentration should shift the conductivity maximum. Samples of SBNx which have varying carrier concentrations have been measured both here and by Dandeneau et al.. Dandeneau found that in SBN0.5 the temperature of the maximum conductivity did not change appreciably, even though the conductivity magnitude changed almost 10 fold [43]. Interestingly, this is not the finding of this work when measuring samples of SBN0.6, where a change in maxima is found with a change in reduction condition. As seen in Figure 3, SBN0.6 samples annealed at 1300°C under $pO_2=10^{-14}$ atm and 10^{-16} atm show maxima at ~680K while samples annealed under $pO_2=10^{-12}$ atm show maxima at ~820K and $pO_2=10^{-10}$ atm have not yet reached a maxima within the measured temperature range. The discrepancy between this work and the work of Dandeneau currently remains an open question. To further investigate the link between the maxima conductivity and the Burns

temperature, further details of the electron transport are needed. To investigate this and the role of the polarization in the proposed carrier freeze-out process, the conductivity and thermopower were studied in more detail.

To elucidate the conduction mechanism in SBN at low temperatures, the natural logarithm of conductivity is plotted versus $T^{-1/4}$ in Figure 4. A linear $\ln(\sigma)\ vs. T^{-1/4}$ behavior is found for temperatures below ~270K, with the onset being slightly dependent on Sr/Ba ratio. This conductivity temperature dependence is suggestive of small polaron hopping at temperatures below $\sim\frac{1}{2}\mathrm{T}_{\mathrm{Debye}}$ as discussed by Emin [44]. At sufficiently high temperatures, small polaron conduction follows the well-known equation $\sigma = \frac{\sigma_o}{T} exp\left(\frac{-E_{Hop}}{kT}\right)$ where E_{Hop} is the activation energy for hopping, but, as small polaron hopping requires interaction with phonons [45], at temperatures below ~$1/2\mathrm{T}_{\mathrm{Debye}}$ the lack of high-energy phonon modes results in $\mathrm{T}^{-1/4}$ behavior. The Debye temperature in SBN was found to be 460K by Henning et al. [46], [47]. $1/2\mathrm{T}_{\mathrm{Debye}}$ is marked on Figure 4 and is shown to correlate with the onset of $\mathrm{T}^{-1/4}$ behavior. This behavior is commonly misinterpreted as variable range hopping as discussed by Emin [45]. At higher temperatures, the conduction should show a linear relationship between $\ln(\sigma T)$ and $1/_{kT}$ with a slope equal to $\mathrm{E}_{\mathrm{Hop}}$. A plot of $ln(\sigma T)\ vs\ 1/_{kT}$ is shown in Figure 5. A line can be fit for a small region between ~300K and 450K for x=0.7 and x=0.6, but the plot clearly becomes nonlinear at higher temperatures. Linear fits for x=0.5 and x=0.4 are not found in any temperature regime. It would seem then that a small polaron picture of conduction may be confined to the low temperature regime of some samples but cannot explain the high-temperature properties.

The divergence from hopping toward metallic-like conduction is similar to trends found in other systems [48–50] for activation to a mobility edge. In this case, a linear decrease in the activation energy with temperature is expected [51]. Assuming a conductivity dependence of $\sigma = \sigma_o exp\left(\frac{-E_\sigma}{kT}\right)$, the differential activation energy is $E_a(T) = \frac{dln(\sigma)}{d(1/_{kT})}$. This calculation was done numerically using the data from Figure 1 and re-plotted in this differentiated form in Figure 6.

The differential activation energy changes linearly with temperature as expected for activation to a mobility edge. The values of $\frac{dE_a}{dT}$, ranging from 2.5×10^{-4} eV/K to 5×10^{-4} eV/K, are similar in magnitude to reports on other materials [48] [52] and comparable in magnitude to the change in band gap with temperature, ~10×10^{-4} eV/K [53], suggesting the temperature dependence of bands is involved. The slope is dependent on the temperature regime. Low temperatures show a positive slope, as is expected for low temperature hopping conduction, or $\ln(\sigma) \propto T^{-1/4}$ behavior. A transition from positive to negative slope is found near 270K and is associated with the transition toward electron activation into bands. More interestingly, changes in $\frac{dE_a}{dT}$ are found near both 450K and 630K. For example, in the x=0.7 sample, there is an increase in $\frac{dE_a}{dT}$ around 630K from 2.2×10^{-4} eV/K to 5×10^{-4} eV/K, and a decrease to 0.3×10^{-4} eV/K below 450K. These transitions are likely associated with the T_{Burns} and the T_f, suggesting that the polarization is playing a role in the activation of electrons into delocalized states. Other samples whose maximum conductivity is near the T_{Burns} show the appearance of a finite $E_a(T)$ value at this point. The increase in $\frac{dE_a}{dT}$ at T_{Burns} suggests the polarization is increasing the activation energy compared to the nonpolar state. Within this model, the activation energy corresponds to activation from the Fermi energy to the mobility edge, and the slope in the nonpolar state is from the temperature dependence of the gap. The mobility edge is present due to the Anderson localization of electrons, the extent of which is dependent on the disorder in the system. Some disorder occurs in the paraelectric phase due to the solid solution of Sr and Ba's as well as oxygen vacancies. Here, we propose that the nanopolar regions are acting as an additional source of disorder. As such, the increase in $\frac{dE_a}{dT}$ below the T_{Burns} is attributed to the disorder from the nanosized domains which grow in number and size as temperature decreases below T_{Burns}. The increased disorder would move the mobility edge away from the E_F and result in a decrease in the electrical conduction due to the increased localization of electrons. If true, once the T_f is reached the polarization would stop influencing the activation energy, and changes in the activation energy would again be controlled by the temperature dependence of the band. This transition occurs and is associated,

for example, with a decrease in $\frac{dE_a}{dT}$ from 5x10^{-4} eV/K to 2.5x10^{-4} eV/K in SBN0.6 at 450K. These decreases in $\frac{dE_a}{dT}$ are not found in SBN0.4 and SBN0.5, suggesting that long-range ordered polarization does not play a similar role. This is thought to be due to the long-range order polarization not causing significant disorder in the system compared to the short-range order of the polarization in the relaxor state.

Further insight can be gained through looking at the thermopower as shown in Figure 7. Specifically, the linear temperature dependence of the thermopower in the normal ferroelectric SBN0.4 sample can be explained by the theory proposed by Cutler and Mott [49]. Cutler and Mott's model finds that for a material where the E_F is surrounded by a finite number of localized states and a mobility edge is located above the E_F, a linear temperature dependence of thermopower is predicted at low temperatures. The thermopower follows $S = \frac{1}{3}\pi^2 \frac{k}{e}\left(kT \frac{dln(\mu_o N)}{dE} - \frac{dE_{Hop}}{dE}\right)\Big|_{E_f}$ where e is the electronic charge, μ_o is the prefactor to the temperature dependence of electron mobility, and N is the density of electronic states. It should be noted that Mott's formula holds only at low temperatures where conductive electrons are only those from localized states, and therefore transport is dominated by hopping behavior. As temperature increases, electrons will be activated above the mobility edge and will quickly dominate conduction due to their higher mobility. If electrons are activated from the valence band above the mobility edge in the conduction band over a gap a $S \propto \frac{1}{T}$ dependence as described in detail by Mott and Davis [51]. If instead the Fermi energy is surrounded by localized states and localized electrons are excited above the mobility edge from around the Fermi energy and not over a gap, a $S \propto \ln(T)$ dependence is expected. Unfortunately, differentiating between a linear dependence and a logarithmic dependence of thermopower requires a larger measurement temperature range then performed in this study and it is not possible to make a clear distinction. Nonetheless a $S \propto \frac{1}{T}$ dependence can be easily ruled out. This scenario is similar to La:$BaTiO_3$ [48] where an impurity band is split into a upper and lower Hubbard subband and

overlaps the empty d-band (which in our case is the Nb 4d t_{2g} band). The E_F then lies at the top of the lower Hubbard sub-band and mobility edges are located above and below as depicted inFigure 8.

As the Sr% increases from SBN0.4 to SBN0.7 a deviation of the thermopower from $\frac{dS}{dT} < 0$ to $\frac{dS}{dT} > 0$ is observed at low temperatures. At higher temperatures samples of all Sr/Ba ratios have their thermopower values converge near $T_{Burns.}$ This suggests that when local polarization is zero, the samples all show similar thermopower behavior. To elucidate what occurs at and above T_{Burns}, a SBN0.6 sample was measured using the Ulvac-Riko ZEM-3 system at NASA Glenn Research Center capable of higher temperature measurements. The measured values are plotted on top of data from the MMR system on Figure 7. The thermopower at temperatures above T_{Burns} seems to be an extension of the behavior found in the normal ferroelectric SBN0.4 sample. This fits with the idea that the increase in $\frac{dE_a}{dT}$ at T_{Burns} is caused by disorder due to the short-range polarization. Once the relaxor ferroelectric SBN0.6 is cooled below T_{Burns}, the disorder from the polarization would cause the mobility edge to move away from E_F and decrease the band carrier concentration. This would result in an increase in the magnitude of the thermopower. If we take this deviation as being due to the short-range order polarization, we can see the trend that emerges within the $(Sr_x,Ba_{1-x})Nb_2O_6$ solid solution. Normal ferroelectric SBN0.4 shows a linear/logarithmic temperature dependence of the thermopower, suggesting that long-range order of the polarization does not affect the Seebeck mechanism appreciably. The more relaxor in character the polarization is, the larger the deviation from this typical behavior. A small deviation is seen in SBN0.5, with the phenomenon increasing in magnitude for SBN0.6 and SBN0.7. The disappearance of this deviation from linear behavior for temperatures greater than the T_{Burns} and for compositions of normal ferroelectric behavior suggests that the relaxor based polarization is strongly correlated to the phenomenon.

Furthermore, the high-accuracy ZEM-3 measurement reveals a small ‘dip’ in the thermopower at 450K which is found on both heating and cooling; the observation was repeated in multiple

measurements. The 450K transition may be due to the onset of immobilization of mesoscale polar nanoregions, as can be seen by the increase in the c/a ratio on cooling in Figure 2. Similar lattice expansions have been found by Paszkowski et al. using the X-ray Bond method [54] for multiple compositions which corroborate dielectric measurements of T_f from Vogel-Fulcher fitting of dielectric data by Huang et al. [40]. The nature of this 'dip' is currently unknown, and warrants further investigation.

Although the proposed model fits most of the data, there are a few concerns to point out. First, in the model, a logarithmic dependence of thermopower is expected at high temperatures. The derivation of this equation for a parabolic band results in a slope of $S\ vs\ ln(T)$ of -298 $\mu V/K^2$. The slope of the measured SBN0.4 sample is notably different: -170 $\mu V/K^2$. This discrepancy could be due to the impurity band not being parabolic. The shape of the band near E_f may be more complicated due to an overlap between the impurity band and conduction band as well as the Hubbard band splitting of the impurity band. Calculations of thermopower within a non-parabolic band are difficult and not widely available. Therefore, it is not essential that the slope of the $S\ vs\ ln(T)$ curve to be -298 $\mu V/K^2$, as predicted for a parabolic band. Another complication arises from the importance of the possible A-site filling during reduction, as implied by the phase-separation of NbO_2 from SBN. As no Ba or Sr-rich phases appear alongside the NbO_2 second phase, the Ba or Sr may enter the naturally present metal vacancies on the A-site. The filling of the A-site may thus play an important role in the disorder of the angles between NbO_6 octahedra and, therefore, perturb d-orbital overlap and subsequently the conduction. These details require further examination, yet are not points which are inconsistent with the current model as a first order approximation. We, therefore, propose that conduction in SBN is via electrons generated from the oxygen vacancy defects. The carriers form an impurity band where the Fermi energy (E_F) lies within localized states in this band. The short-range order of relaxor ferroelectric SBN seems to act as a source of disorder, affecting the mobility edge and therefore the activation energy of electrons into delocalized states.

These results do not suggest ferroelectric polarization completely suppresses metallic conduction, but can act as a source of disorder which may localize carriers if the bandwidth is low. This model suggests there is a tradeoff when using a relaxor ferroelectric as a thermoelectric. The relaxor ferroelectric polarization causes a low thermal conductivity but can also decrease high mobility carrier density by localizing electrons due to Anderson localization. One should then aim to have sufficient d-orbital overlap so the bandwidth is large and carriers are more difficult to localize. A higher total carrier concentration would also suppress localization in the impurity band, but too high of a carrier concentration could lead toward thermopower becoming too low to be effective as a thermoelectric. This balance is found in SBN once carriers are delocalized at high temperatures as indicated by the high power factor along the c-axis, but localization limits usefulness below ~500K. Nevertheless, the low thermal conductivity coupled with the high-temperature power factor lead toward the high figure of merit.

Conclusions

Electrical conductivity and thermopower measurements of different Sr/Ba ratios of SBN were used to study the conduction mechanism. Proposed here is a model where the E_F is surrounded by a finite number of localized electronic states that are separated from delocalized states via a mobility edge. This mechanism results in hopping conduction at low temperatures, consistent with the observed $T^{-1/4}$ behavior. The thermopower of samples with normal ferroelectric behavior fit the model proposed by Cutler and Mott for a Fermi energy surrounded by localized states, and the temperature dependent activation energies shows linear dependences consistent with an activation from the Fermi energy to a mobility edge varying with temperature.

Acknowledgements

This study was supported in part by BSF Grant No. 2011510 and NSF Grant No. 0120812. Use of the Advanced Photon Source, an Office of Science User Facility operated for the U.S. Department of

Energy (DOE) Office of Science by Argonne National Laboratory, was supported by the U.S. DOE under Contract No. DE-AC02-06CH11357. The authors also acknowledges Dr. Alp Sehirlioglu and Jon Mackey at NASA Glenn Research Center for help and use of the ZEM-3 thermoelectric measurement system.

References

[1] K. Uchino, *Ferroelectric Devices* (Marcel Dekker, Inc., New York, NY, 2000).

[2] P. Muralt, R. G. Polcawich, and S. Trolier-McKinstry, MRS Bull. **34**, (2009).

[3] N. Setter, D. Damjanovic, L. Eng, G. Fox, S. Gevorgian, S. Hong, A. Kingon, H. Kohlstedt, N. Y. Park, G. B. Stephenson, I. Stolitchnov, A. K. Taganstev, D. V. Taylor, T. Yamada, and S. Streiffer, J. Appl. Phys. **100**, 051606 (2006).

[4] R. Thomas, J. F. Scott, D. N. Bose, and R. S. Katiyar, J. Phys. Condens. Matter **22**, 423201 (2010).

[5] R. Whatmore, Reports Prog. Phys. **49**, 1335 (1986).

[6] R. E. Jones, P. D. Maniar, R. Moazzami, P. Zurcher, J. Z. Witowski, Y. T. Lii, P. Chu, and S. J. Gillespie, Thin Solid Films **270**, 584 (1995).

[7] G. Lewis, J. Am. Ceram. Soc. **58**, 555 (1985).

[8] S. Y. Yang, J. Seidel, S. J. Byrnes, P. Shafer, C.-H. Yang, M. D. Rossell, P. Yu, Y.-H. Chu, J. F. Scott, J. W. Ager, L. W. Martin, and R. Ramesh, Nat. Nanotechnol. **5**, 143 (2010).

[9] H. Huang, Nat. Photonics **4**, 134 (2010).

[10] V. Fridkin and B. Popov, Sov. Phys. Uspekhi **21**, 981 (1978).

[11] S. Lee, G. Yang, R. Wilke, S. Trolier-McKinstry, and C. A. Randall, Phys. Rev. B **79**, 134110 (2009).

[12] S. Lee, R. H. T. Wilke, S. Trolier-McKinstry, S. Zhang, and C. A. Randall, Appl. Phys. Lett. **96**, 031910 (2010).

[13] S. Lee, S. Dursun, C. Duran, and C. A. Randall, J. Mater. Res. **26**, 26 (2011).

[14] S. Lee, J. A. Bock, S. Trolier-McKinstry, and C. A. Randall, J. Eur. Ceram. Soc. **32**, 3971 (2012).

[15] J. Seidel, L. W. Martin, Q. He, Q. Zhan, Y.-H. Chu, A. Rother, M. E. Hawkridge, P. Maksymovych, P. Yu, M. Gajek, N. Balke, S. V Kalinin, S. Gemming, F. Wang, G. Catalan, J. F. Scott, N. A. Spaldin, J. Orenstein, and R. Ramesh, Nat. Mater. **8**, 229 (2009).

[16] T. Sluka, A. K. Tagantsev, D. Damjanovic, M. Gureev, and N. Setter, (2012).

[17] R. K. Vasudevan, W. Wu, J. R. Guest, A. P. Baddorf, A. N. Morozovska, E. A. Eliseev, N. Balke, V. Nagarajan, P. Maksymovych, and S. V. Kalinin, Adv. Funct. Mater. **23**, 2592 (2013).

[18] M. Schröder, A. Haußmann, A. Thiessen, E. Soergel, T. Woike, and L. M. Eng, Adv. Funct. Mater. **22**, 3936 (2012).

[19] T. Sluka, A. K. Tagantsev, P. Bednyakov, and N. Setter, Nat. Commun. **4**, 1808 (2013).

[20] J. Guyonnet, I. Gaponenko, S. Gariglio, and P. Paruch, Adv. Mater. **23**, 5377 (2011).

[21] T. Kolodiazhnyi, M. Tachibana, H. Kawaji, J. Hwang, and E. Takayama-Muromachi, Phys. Rev. Lett. **104**, 147602 (2010).

[22] T. Kolodiazhnyi, Phys. Rev. B **78**, 045107 (2008).

[23] I. Sergienko, V. Keppens, M. McGuire, R. Jin, J. He, S. Curnoe, B. Sales, P. Blaha, D. Singh, K. Schwarz, and D. Mandrus, Phys. Rev. Lett. **92**, 065501 (2004).

[24] Y. Shi, Y. Guo, X. Wang, A. J. Princep, D. Khalyavin, P. Manuel, Y. Michiue, A. Sato, K. Tsuda, S. Yu, M. Arai, Y. Shirako, M. Akaogi, N. Wang, K. Yamaura, and A. T. Boothroyd, Nat. Mater. **12**, 1024 (2013).

[25] I.-K. Jeong, S. Lee, S.-Y. Jeong, C. Won, N. Hur, and A. Llobet, Phys. Rev. B **84**, 064125 (2011).

[26] P. W. Anderson and E. I. Blount, Phys. Rev. Lett. **14**, 217 (1965).

[27] B. T. Matthias, J. Appl. Phys. **38**, 928 (1967).

[28] M. Tachibana, T. Kolodiazhnyi, and E. Takayama-Muromachi, Appl. Phys. Lett. **93**, 092902 (2008).

[29] P. E. Hopkins, C. Adamo, L. Ye, B. D. Huey, S. R. Lee, D. G. Schlom, and J. F. Ihlefeld, Appl. Phys. Lett. **102**, 121903 (2013).

[30] J. Hlinka, S. Kamba, J. Petzelt, J. Kulda, C. Randall, and S. Zhang, Phys. Rev. Lett. **91**, 107602 (2003).

[31] O. Delaire, J. Ma, K. Marty, A. May, and M. McGuire, Nat. Mater. **10**, 614 (2011).

[32] A. A. Bokov and Z.-G. Ye, J. Mater. Sci. **41**, 31 (2006).

[33] L. E. Cross, Ferroelectrics **76**, 241 (1987).

[34] E. Fischer, W. Hässler, and E. Hegenbarth, Phys. Status Solidi **169**, 69 (1982).

[35] C. L. Choy, W. P. Leung, T. G. Xi, Y. Fei, and C. F. Shao, J. Appl. Phys. **71**, 170 (1992).

[36] H. Lee and R. Freer, J. Mater. Sci. **33**, 1703 (1998).

[37] N. E. Brown, S. M. Swapp, C. L. Bennett, and A. Navrotsky, J. Appl. Crystallogr. **26**, 77 (1993).

[38] A. S. Bhalla, R. Guo, L. E. Cross, G. Burns, F. H. Dacol, and R. R. Neurgaonkar, Phys. Rev. B **36**, 2030 (1987).

[39] A. Bhalla, R. Guo, L. Cross, G. Burns, F. H. Dacol, and R. R. Neurgaonkar, J. Appl. Phys. **71**, 5591 (1992).

[40] W. H. Huang, D. Viehland, and R. R. Neurgaonkar, J. Appl. Phys. **76**, 490 (1994).

[41] V. Shvartsman, W. Kleemann, T. Łukasiewicz, and J. Dec, Phys. Rev. B **77**, 054105 (2008).

[42] K. Kobayashi, Y. Kato, Y. Katayama, and K. F. Kamatsubara, Phys. Rev. … **37**, 772 (1976).

[43] C. S. Dandeneau, T. W. Bodick, R. K. Bordia, and F. S. Ohuchi, J. Am. Ceram. Soc. **96**, 2230 (2013).

[44] D. Emin, Phys. Rev. Lett. **32**, 303 (1974).

[45] D. Emin, Phys. Rev. B **15**, 3667 (1977).

[46] I. Henning, M. Mertig, R. Plath, G. Pompe, E. Heganbarth, and R. Schalge, Phys. Status Solidi **73**, K105 (1982).

[47] S. Liu and L. Cross, Phys. Status Solidi **41**, K83 (1977).

[48] S. R. Gilbert, L. A. Wills, B. W. Wessels, J. L. Schindler, J. A. Thomas, and C. R. Kannewurf, J. Appl. Phys. **80**, 969 (1996).

[49] M. Cutler and N. F. Mott, Phys. Rev. **181**, 1336 (1969).

[50] M. Cutler, J. Leavy, and R. Fitzpatrick, Phys. Rev. **133**, A1143 (1964).

[51] N. F. Mott and E. A. Davis, *Electronic Processes in Non-Crystalline Materials*, 2nd ed. (Oxford University Press, Oxford, 1979).

[52] J. T. Edmond, Brit. J. Appl. Phys. **17**, 979 (1966).

[53] C. David, a. Tunyagi, K. Betzler, and M. Wöhlecke, Phys. Status Solidi **244**, 2127 (2007).

[54] R. Paszkowski, K. Wokulska, T. Łukasiewicz, and J. Dec, Cryst. Res. Technol. **48**, 413 (2013).

FIGURES

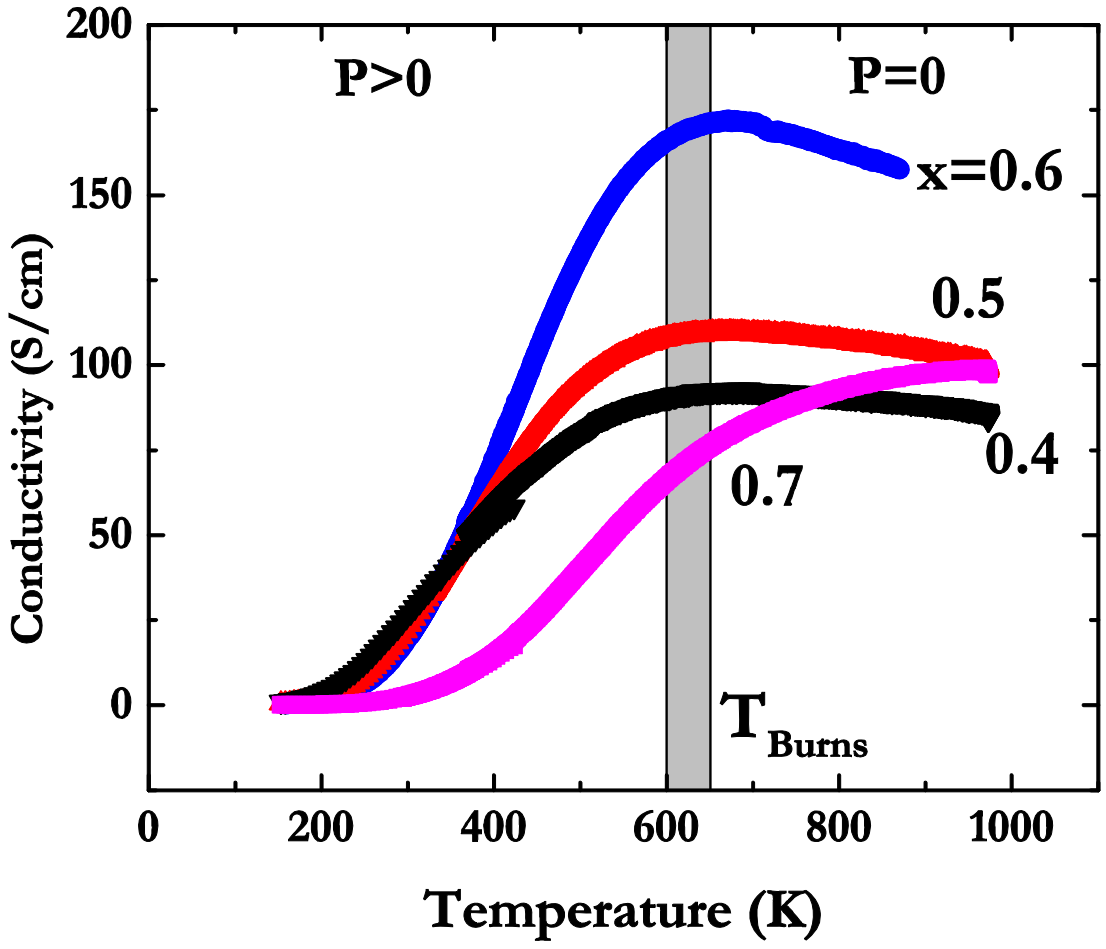

Figure 1. Electrical conductivity of $(Sr_x,Ba_{1-x})Nb_2O_{6-\delta}$ from 150K to 1000K. Measurements at temperatures greater than ~450K were performed under a reducing atmosphere consistent with the pO_2 used during sample annealing. Maxima for x=0.4-0.6 are located near T_{Burns}, while x=0.7 has a maxima shift to higher temperatures.

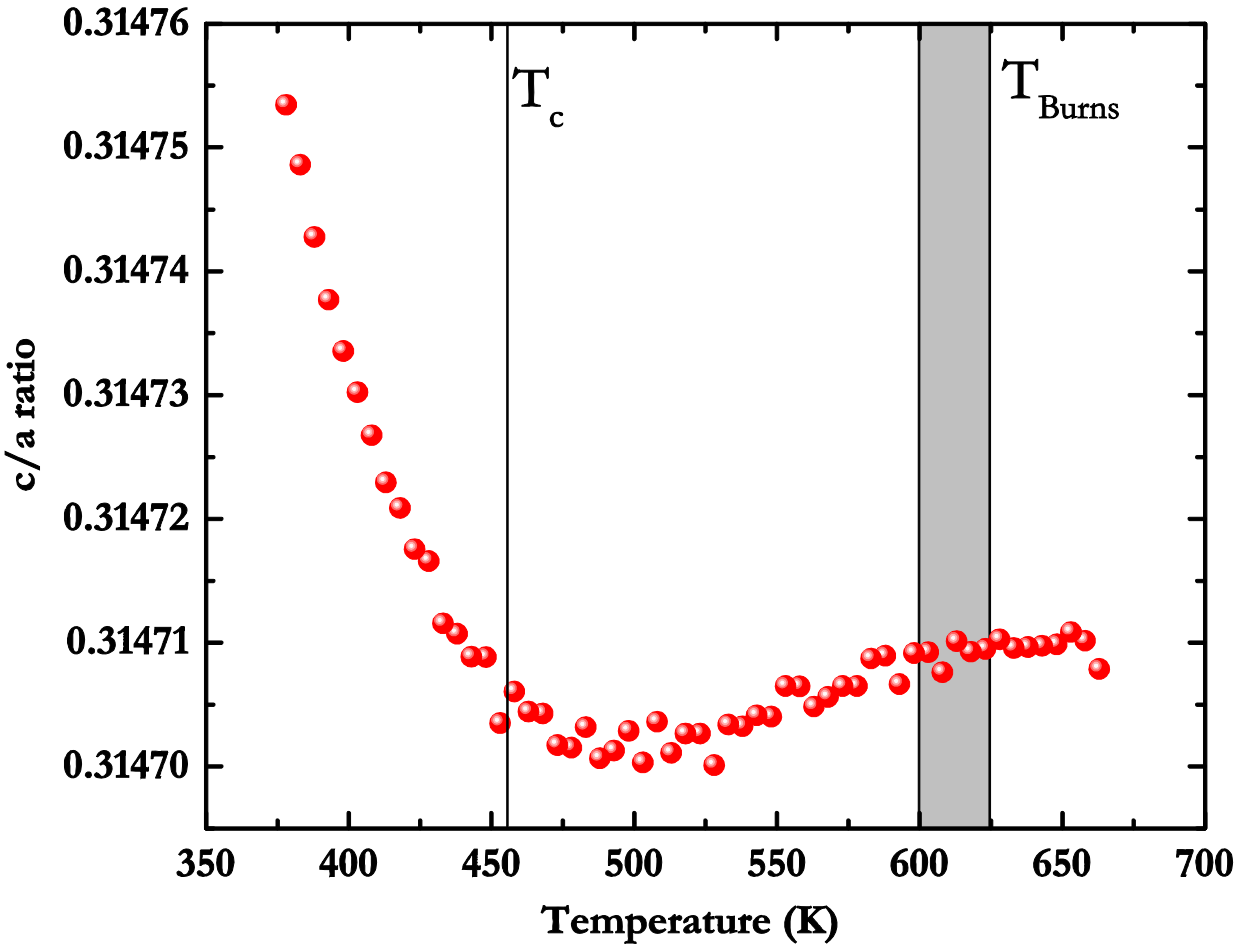

Figure 2. c/a ratio of a x=0.6 sample from 375K to 660K. A linear dependence is seen >~625K, suggesting paraelectric behavior; a decrease in c/a ratio is due to the short-order polarization between 450K and 625K, and an increase is found <450K associated with the freezing in of mesoscale polar nano-regions

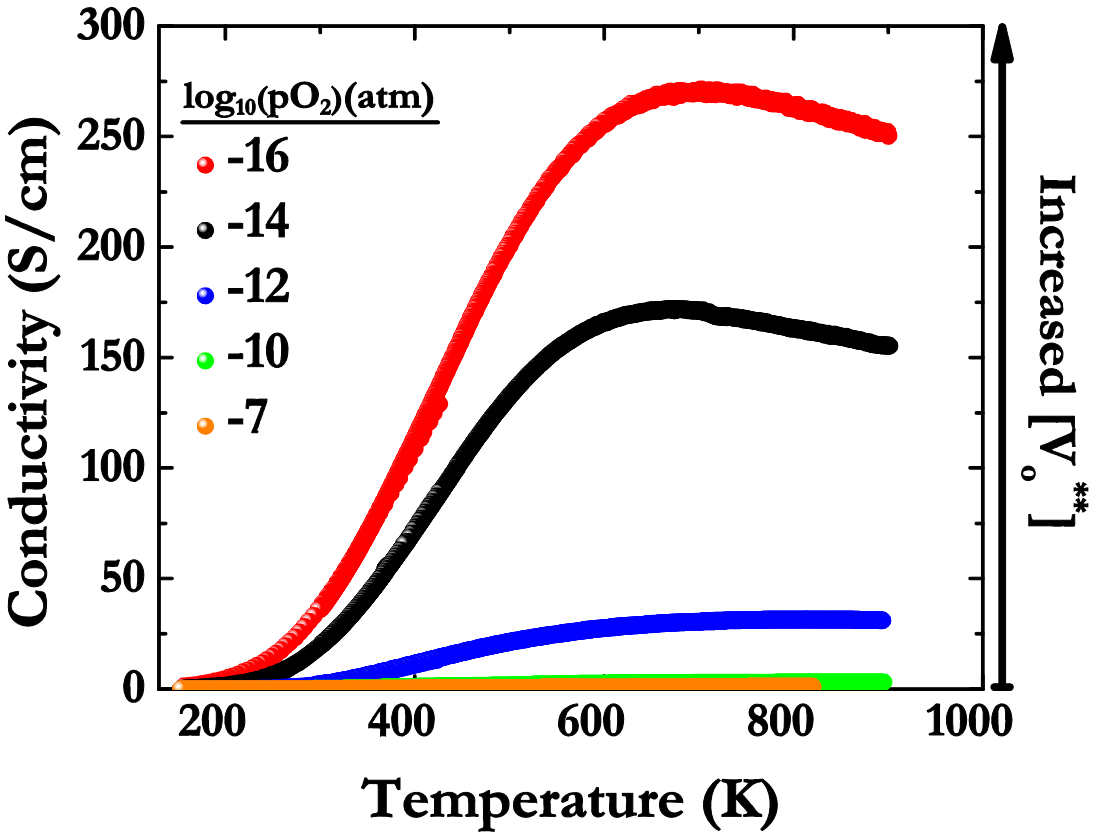

Figure 3. $(Sr_{0.6},Ba_{0.4})Nb_2O_{6-\delta}$ annealed under partial pressures of oxygen ranging from $pO_2=10^{-7}$ to 10^{-16}. Maxima in conductivity shift depending on reduction condition.

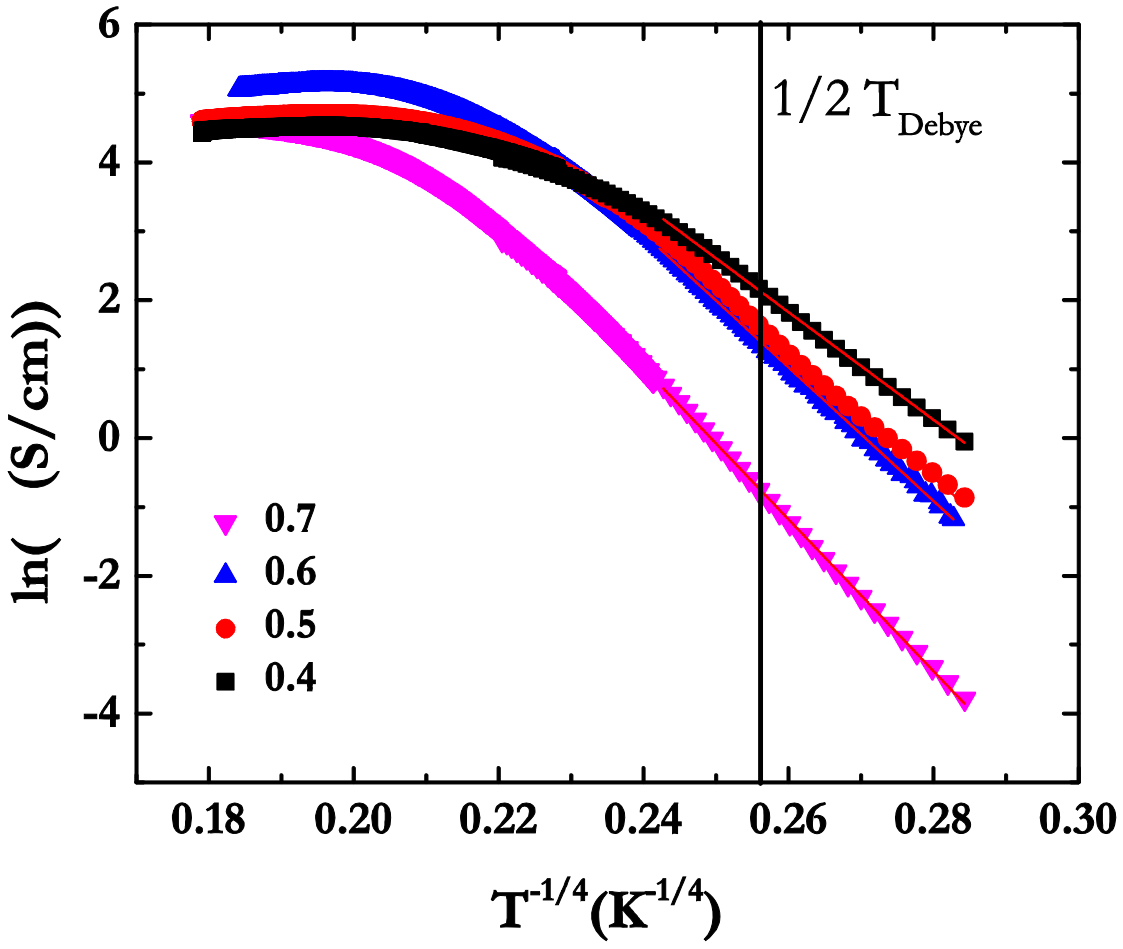

Figure 4. $T^{-1/4}$ behavior of the conductivity is found below ~270K. Emin [44] suggests this may be due to loss of multiphonon hopping processes below ~$1/2T_{Debye.}$ The values for $1/2T_{Debye}$ for x=0.6 SBN found by Henning [46] is plotted and correlates qualitatively well with the onset of $T^{-1/4}$ behavior.

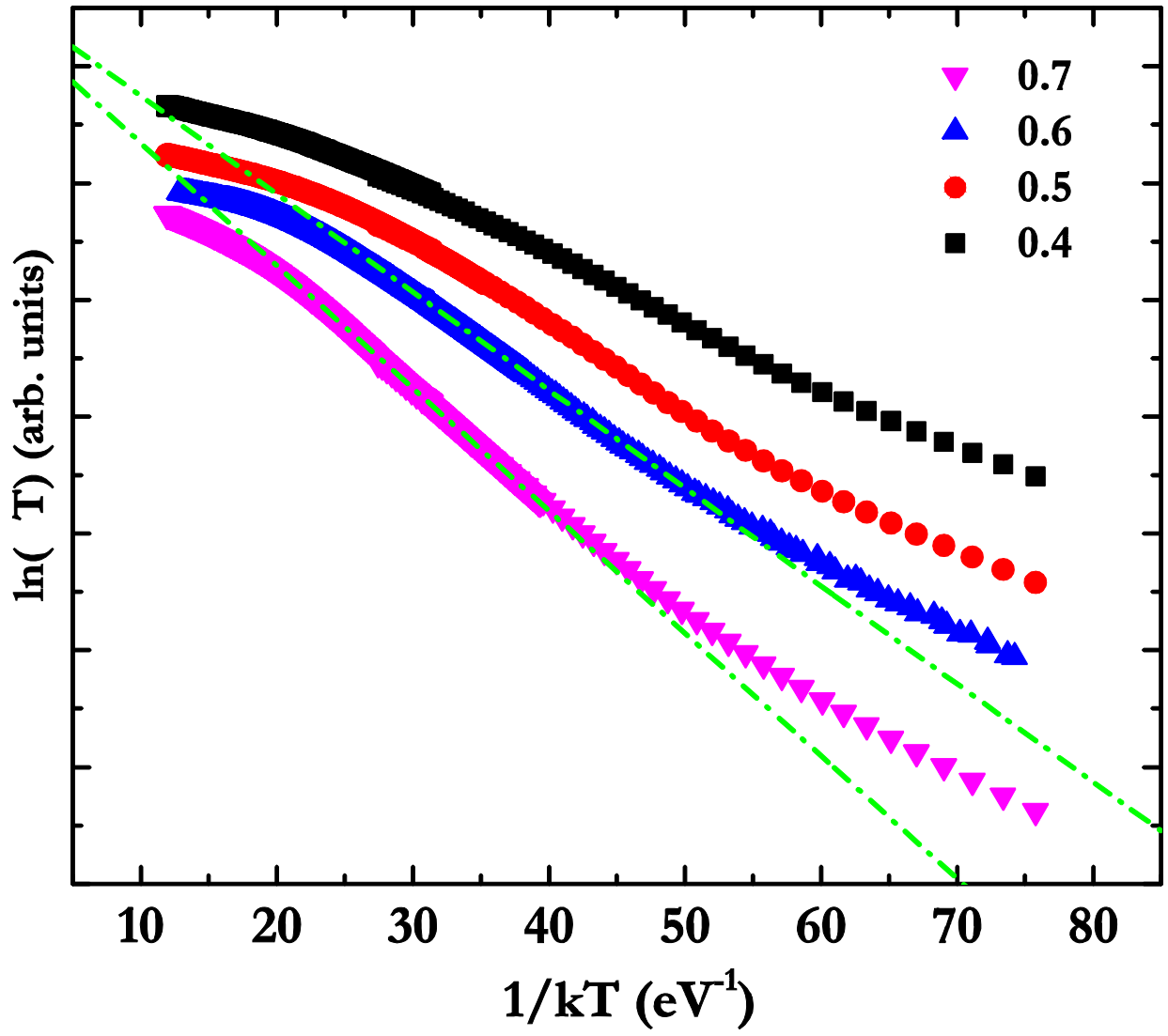

Figure 5. Natural log of electrical conductivity-temperature product plotted against reciprocal thermal energy. Linear dependence is expected for small polaron controlled conduction. Areas of x=0.7 and 0.6 samples are linear, suggesting this mechanism. High and low temperatures deviate from this dependence.

.

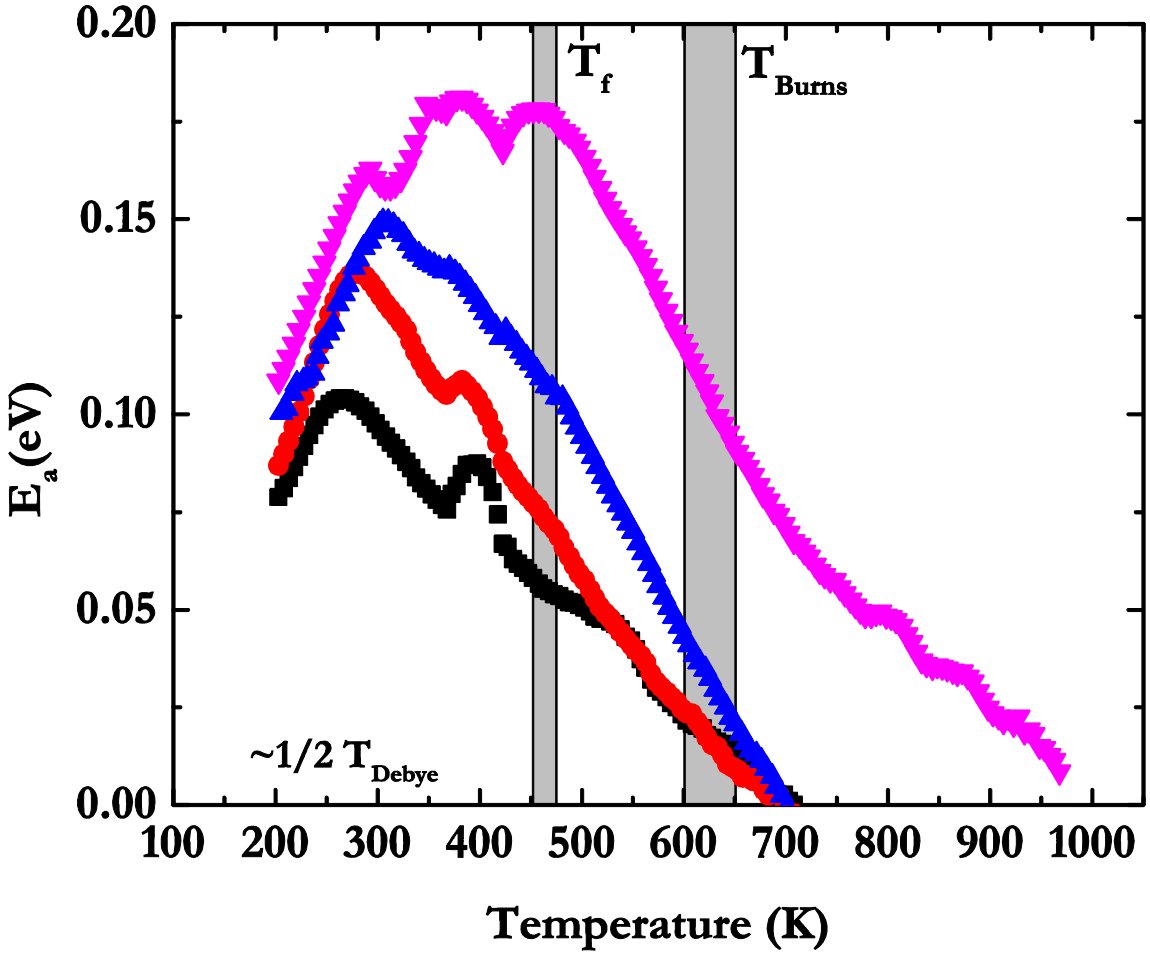

Figure 6. Temperature dependent activation energies calculated from conductivity data. Changes in slope are found at 450K and 625K associated with the changes in polarization in the sample, as discussed in the text.

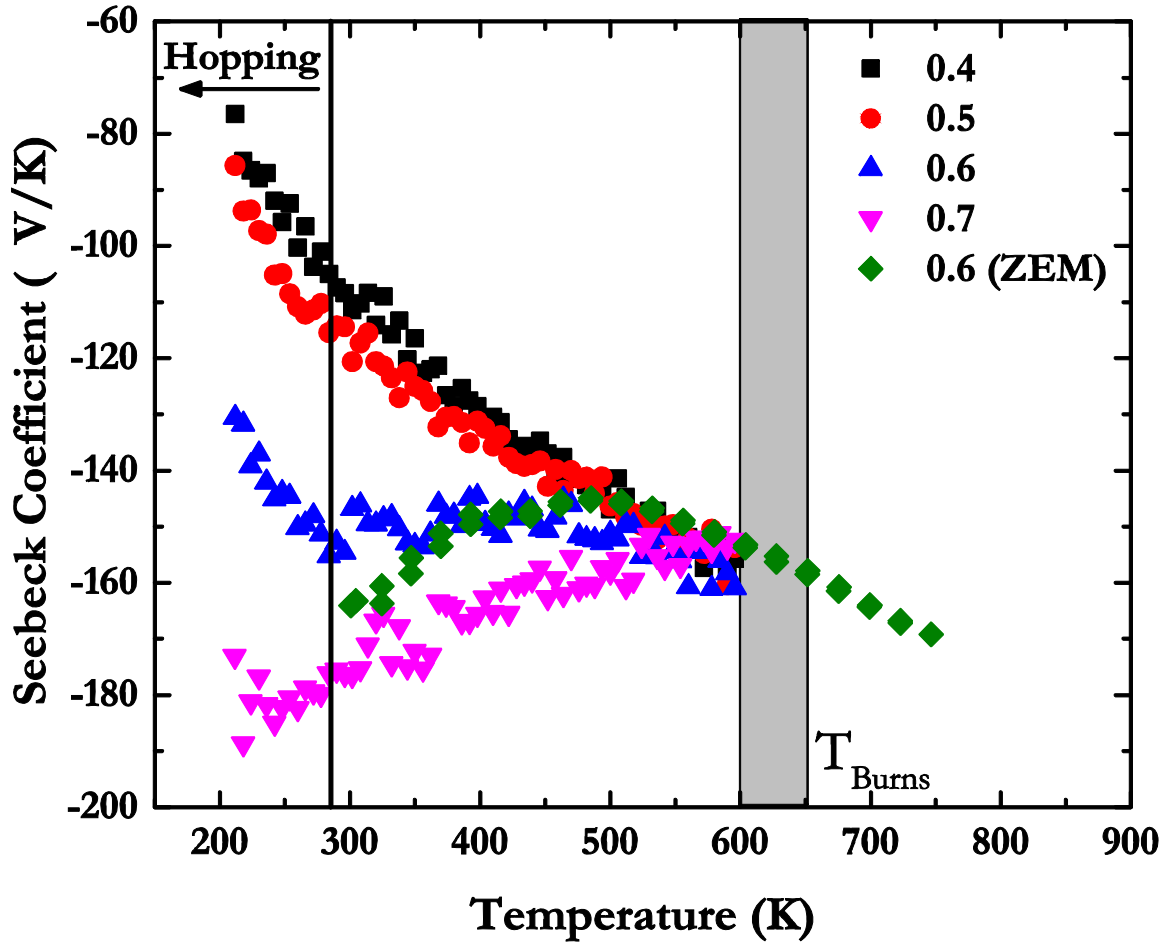

Figure 7. Thermopower of $(Sr_x,Ba_{1-x})Nb_2O_{6-\delta}$ from 200K to 600K and an x=0.6 sample measured from room temperature to 750K. Thermopower of all samples coincide at the Burns temperature, and the x=0.6 sample shows to continue the trend of the normal ferroelectric x=0.4 and x=0.5 samples above the Burns temperature. This suggests that the nonlinearity found in the x=0.6 and x=0.7 samples is due to the short-range order polarization.

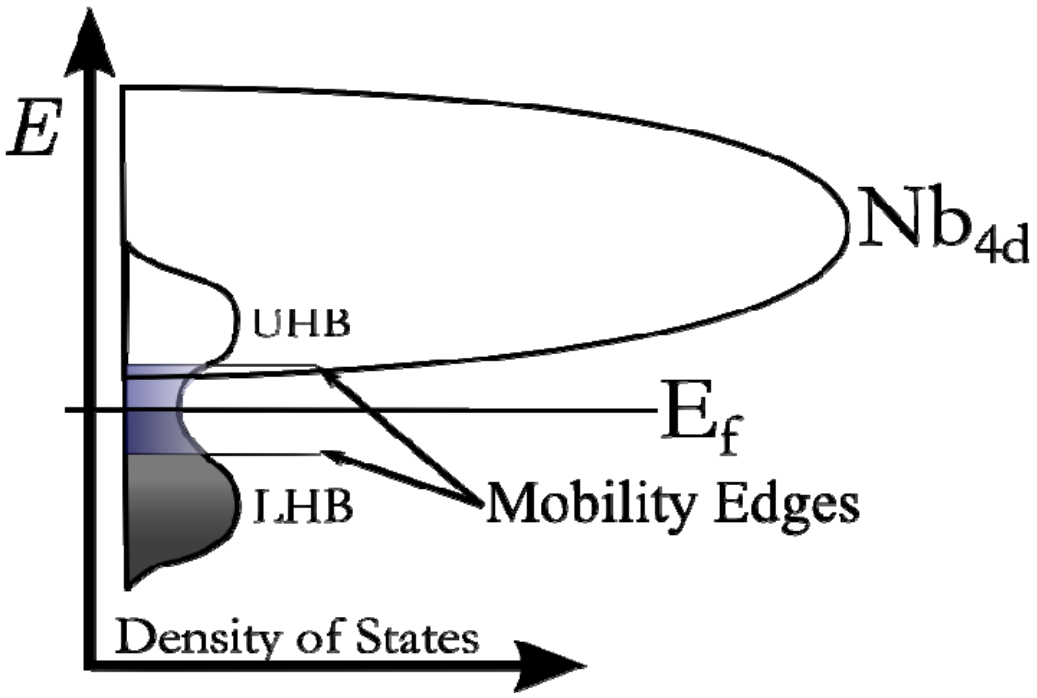

Figure 8. Proposed density of states for oxygen deficient Strontium Barium Niobate. Oxygen deficiency creates an impurity band which splits into upper (UHB) and lower (LHB) Hubbard sub-bands. The Fermi energy is located between the upper and lower sub-bands within localized states which are separated from delocalized states via a mobility edges as shown.